Hindawi
International Journal of Chemical Engineering
Volume 2022, Article ID 7355170, 10 pages
https://doi.org/10.1155/2022/7355170

Research Article

Improving Catalytic Activity and Thermal Stability of Methyl-Parathion Hydrolase for Degrading the Pesticide of Methyl-Parathion

Cheng Shi,[1,2,3] **Song Liu**,[1,2,3] **and Guocheng Du**[1,2,3,4]

[1]*National Engineering Research Center for Cereal Fermentation and Food Biomanufacturing, Jiangnan University, Wuxi 214122, China*
[2]*Science Center for Future Foods, Jiangnan University, Wuxi 214122, China*
[3]*School of Biotechnology, Jiangnan University, Wuxi 214122, China*
[4]*The Key Laboratory of Carbohydrate Chemistry and Biotechnology, Ministry of Education, Jiangnan University, Wuxi 214122, China*

Correspondence should be addressed to Guocheng Du; gcdu@jiangnan.edu.cn

Received 24 January 2022; Accepted 7 March 2022; Published 6 April 2022

Academic Editor: G.L. Balaji

Pesticides are indispensable in today's agriculture. Methyl-parathion hydrolase (MPH, E.C.3.1.8.1) could hydrolyze organophosphorus pesticides, including methyl-parathion. MPH could rehabilitate soil and water resources contaminated by organophosphorus pesticides. However, natural MPHs generally exhibited a low tolerance to high temperatures and low catalytic efficiency. In this study, we improved the catalytic efficiency toward methyl-parathion and the thermal stability of the MPH from *Pseudomonas* sp. WBC-3 through saturation mutagenesis and fusion with self-assembling amphipathic peptides (SAP). The experimental characterization showed that compared to the wild-type enzyme, the k_{cat}/K_m of the mutant T271S yielded by saturation mutagenesis was increased by 224.3% compared to the wild-type MPH. T_{50} and T_m of SAP3-MPH with an SAP fused at the N-terminus were increased by 6.2°C and 6.0°C, respectively. Compared to the wild-type enzyme, T271S fused with SAP3 at the N-terminus (SAP3-T271S) exhibited a 2.1-fold increase in k_{cat}/K_m without significantly affecting the thermal stability. The simultaneous improvement of the catalytic efficiency and thermal stability of MPH would be beneficial for its application in the degradation and detection of organophosphorus pesticides. Furthermore, our study provides a potential combination strategy for the design of the other enzyme preparations of pollutant degradation.

1. Introduction

The large-scale use of pesticides causes the pollution of water and soil resources [1, 2]. Methyl-parathion hydrolase (MPH, E.C.3.1.8.1) could catalyze the hydrolysis of methyl-parathion and other organophosphorus pesticides [3]. By converting to small molecules that are less toxic to mammals, MPH shows the application potential for remediating those soil and water contaminated by organophosphorus pesticides in addition to the use as a core component of fruit and vegetable detergents [4]. The degradation product (nitrophenol) solution is yellow in an alkaline environment and has an absorption peak at 405 nm [5]. Based on these features, MPH has been applied to construct enzyme-linked sensors for quantitatively detecting methyl-parathion content [6]. To date, MPH has been isolated from *Pseudomonas* sp. WBC-3 [3], *Plesiomonas* sp. M6 [7], *Stenotrophomonas* sp. SMSP-1 [8], *Burkholderia Jiangsuensis* MP-1 [9], etc. However, natural MPHs generally exhibited a low tolerance to high temperatures [10, 11], and it is thus necessary to improve their catalytic efficiency and stability.

The thermal stability and catalytic efficiency of MPH have been modified by semirational design, directed evolution, or immobilization. As indicated by the crystal structure, MPH belongs to the β-lactam family, many members of which have been well studied [3, 12]. Based on

homologous amino acid sequence analysis, MPH from *Burkholderia Jiangsuensis* MP-1 was modified through a conserved residue substitution, yielding the mutant T64N with a 5.9-fold increase in k_{cat}/K_m [9]. Proline substitution within the flexible region enhanced the half-inactivation temperature (T_{50}) of MPH from *Ochrobactrum* SP. M231 was increased by 2.7°C [13]. Moreover, the transcription factor DmpR that is activated by organophosphorus degradation products enabled the high-throughput detection of the MPH activity based on the signal of fluorescent protein [14]. By using this system, the mutant with a 100 times increase in k_{cat}/K_m *p*-nitrophenyl diphenyl phosphate was finally isolated from the mutant library of *Pseudomonas* sp. strain CF600 MPH [14]. In addition, the thermal stability of *Pseudomonas stutzeri* ZK-5 MPH was remarkably enhanced when it is immobilized using cross-linked poly (γ-glutamic acid)/gelatin hydrogel [11]. However, the rational design based on enzyme-substrate interaction analysis was rare for MPH activity enhancement.

The improvement in computing power makes full use of structural information to predict the key residues for enzymatic reactions [15]. The affinity between an enzyme and a substrate/inhibitor can be quantified using binding free energy [16, 17]. Despite the sacrifice of some precision, the method based on the master equation can rapidly assess the binding free energy [18]. The virtual amino acid mutation based on this method has been used to engineer the ω-transaminase, resulting in an 8.5 times increase in its catalytic efficiency [19]. In our previous study, we first reported the enhancement of enzyme thermal stability by fusing with self-assembling amphipathic peptides (SAP) [20]. By optimizing the SAP and linker sequence, the SAP fusion increased the half-life of polygalacturonate lyase, lipoxygenase, and L-asparaginase by 33.25-, 17.55- and 15.6-fold, respectively, compared to the corresponding wild-type enzyme [21]. To be noted, the SAP fusion generally showed little or even positive impact on the enzyme activity [20, 21]. Thus, the combination of virtual mutation and SAP fusion may be a feasible method to simultaneously improve the catalytic efficiency and thermal stability of an enzyme.

In this study, the catalytic efficiency of the MPH from *Pseudomonas* sp. WBC-3 toward methyl-parathion was improved by modifying the critical residues, which were predicted using the virtual mutation based on binding free energy change. Then, the thermal stability of the MPH was enhanced by fusing SAP at the terminus. The mechanism for the enhanced catalytic efficiency was analyzed based on molecular dynamics.

2. Materials and Methods

2.1. Strains and Plasmids. *E. coli* JM109 (Novagen, Madison, WI, USA) was used for gene cloning. *E. coli* BL21 (DE3) (Novagen, Madison, WI, USA) and the plasmid pET-28a (+) (Novagen, USA) were used for the expression of MPH and its mutants.

2.2. Plasmid Construction. Each gene expressing the wild-type MPH or its mutants with a C-terminal 10×His tag was inserted into the expression plasmid pET-28a (+). In order to express the wild-type MPH with a 10×His tag, the gene of the MPH was amplified from the genome of *Pseudomonas* sp. WBC-3 by PCR using the primer pairs (28a)-mph-his10-F and (28a)-mph-his10-R as the sense and antisense primers, respectively. The plasmid pET-28a (+) was linearized by the primer pairs (28a)-F and (28a)-R. Then the amplified DNA expressing the wild-type MPH with a C-terminal 10×His tag was inserted into the linearized plasmid pET-28a (+) to generate the plasmid pET-28a/mph-his10, which was based on a one-step cloning method by the ClonExpress II One Step Cloning Kit (Vazyme, Nanjing, China). The saturated mutant libraries of MPH and the combinatorial mutant D151E/T271S/L273 were accomplished using the MutanBEST Kit (Takara, Dalian, China) according to the manufacturer's manual with the plasmid pET-28a/mph-his10 as the template. All the primer pairs used here are listed in Table S1. All the plasmids were transformed into *E. coli* BL21 (DE3) for protein expression.

The plasmid expression MPH fused with an N-terminal SAP was yielded by linking the linearized plasmid pET-28a/mph-his10 and an SAP with homologous arms according to the ClonExpress II One Step Cloning Kit. The linearized plasmid pET-28a/mph-his10 was amplified by the primer pairs (pt)-mpd-F and (pt)-28a-R, while the SAP with homologous arms was amplified by primer pairs listed in Table S1. The homologous arms of each amplified SAP were 5′-AGAAGGAGATATACCATG-3′ and 5′-CCGACGCCGCCAACCACC-3′. The plasmid expression MPH fused with an SAP at the C-terminal was constructed by a similar flow. The difference was that the homologous arms were 5′-AGAAGGAGATATACCATG-3′ and 5′-CCGACGCCGCCAACCACC-3′, and the primer pairs to amplify pET-28a/mph-his10 were (pt)-28a-F and (pt)-mph-R (Table S1). The plasmids expressing SAP3-T271S were accomplished with the plasmid pET-28a/sap3-mph-his10 as the template through single-point mutation according to the manufacturer's manual of the MutanBEST Kit (Takara, Dalian, China). All the primer pairs used here are listed in Table S1. All the plasmids were transformed into *E. coli* BL21 (DE3) for protein expression.

2.3. The Library Screening of Mutants. In the primary screening process, the seeds of the single-point and double-point saturated mutant libraries for MPH were cultured in a Luria-Bertani medium containing 50 μg/ml kanamycin in 96-well plates. After overnight cultivation at 37°C, 1% (v/v) *E. coli* seed cultures were transferred into a Luria-Bertani medium containing 50 μg/ml kanamycin at 37°C for 2 h. Then protein production was induced by the addition of isopropyl-β-D-thiogalactopyranoside (IPTG) at a final concentration of 1 mM at 37°C for 4 h. The cells were centrifuged and resuspended in phosphate buffer (20 mM, pH 7.0), which was repeated three times. After each resuscitation, the cells were dialyzed for 30 minutes. Then, the cells were freeze-thawed 3 times at −80°C for 1 minute and

37°C for 2 minutes. The positive mutation satisfied the condition that the special activity of the MPH mutant in the crude enzyme fluid was at least 30% higher than that of the wild-type MPH. The specific enzyme activity of the crude enzyme fluid was calculated by an approximate formula:

$$v_{\text{special}} = \frac{v_{\text{OD}}}{m_{\text{OD, MPH}} - m_{\text{OD,blank}}}, \quad (1)$$

where v_{special} is the special enzyme activity of wild-type MPH or its mutants in the crude enzyme fluid. v_{OD} is the specific enzyme activity of unit OD of the crude enzyme fluid. $m_{\text{OD, MPH}}$ is the total protein concentration of unit OD of the strain expressing wild-type MPH or mutants. $m_{\text{OD, blank}}$ is the total protein concentration of unit OD of the strain containing the empty vectors pET-28a (+).

2.4. Protein Expression and Purification. In the rescreening process, a single colony of each recombinant *E. coli* strain obtained from the primary screening was inoculated into a Luria-Bertani medium containing kanamycin (50 μg/ml) for seed culture at 37°C overnight. Then, the seed culture broth was transferred into Terrific Broth with kanamycin (50 μg/ml) and grown at 37°C. When the optical density of the culture at 600 nm reached 0.6, the protein production was induced by the addition of isopropyl-β-D-thiogalactopyranoside (IPTG) at a final concentration of 1 mM at 20°C for 14 h. After centrifugation, the cells were resuspended in phosphate buffer (20 mM, pH 7.4) and wall-broken by a high-pressure homogenizer (Union-Biotech, Shanghai, China) at 80 MPa for 30 s. The cell lysis buffer was subjected to affinity purification using the HisTrap HP column (GE Healthcare, USA), and the recombinant MPH or its mutants were eluted with 300 mM imidazole in phosphate buffer (20 mM, pH 7.4). After desalting on the HisTrap Desalting column (GE Healthcare, USA), the purified proteins were ready for the MPH activity assay. The protein expression and purification of MPH fused with an SAP were the same as above.

2.5. Enzyme Characterization. The dynamic thermal stabilities of MPH and MPH-SAP fusions were investigated by measuring the residual activity after incubating the enzyme solution in 100 mM Tris-HCl (pH 9). The half-temperature of heat inactivation (T_{50}) was calculated by fitting the residual activity after incubating for 10 min at different temperatures from 20 to 80°C.

The thermodynamic stability parameter of melting temperature (T_{m}) was performed on a Q2000 nano differential scanning calorimeter (TA, Waters, USA). MPH and MPH-SAP fusions (200 μg/ml) were equilibrated for 10 min at 0°C. The unfolding process of proteins was observed at 0–100°C with a scan rate of 2°C/min. T_{m} values and the enthalpy changes of the protein denaturation process were calculated by the deconvolution analysis through a non-two-state model.

Apparent kinetic parameters (K_{m} and k_{cat}) were measured in 100 mM Tris-HCl (pH 9) using methyl-parathion ranging from 15 to 120 μM or ethyl-parathion ranging from 12 to 90 μM. All the experiments were repeated three times, and the kinetic parameters were evaluated by the nonlinear fitting of the Michaelis–Menten equation.

2.6. Enzyme Activity Assays. The MPH enzyme activity assay was accomplished according to a previous study with a certain modification [22]. The MPH enzyme reaction was performed at 35°C in a final reaction volume of 3.2 ml containing 100 mM Tris-HCl (pH 9), 120 μM methyl-parathion, or 90 μM ethyl-parathion, and 240 ng/ml MPH. One unit of the enzyme was defined as the amount of the MPH that catalyzed the conversion of 1 μmol methyl-parathion or ethyl-parathion per minute at 35°C. Protein concentration was measured by the BCA protein assay kit (Tiangen Biotech, China).

2.7. Structure Analysis. Circular dichroism (CD) and fluorescence spectroscopy analysis were done according to a previous study [20]. CD analysis was accomplished by continuously collecting the ellipticity data of enzymes in the far-UV CD band of 190–250 nm MOS-450/AF-CD-STP-A (Bio-Logic, France). Fluorescence spectroscopy was monitored at 300–400 nm and excited at 280 nm.

2.8. Docking Analysis. The structure of MPH (PDB: 1P9E) was prepared by Discovery Studio standard procedures, and then hydrogen atoms of histidine interacting with Zn^{2+} were deleted. The docking between MPH and the substrate was completed by CDOCKER of Discovery Studio (https://www.3ds.com/). The radius for pose clustering to increase the diversity of docked poses was 0.1 Å. The number of rotated ligand orientations to refine for each of the conformations was 20. Other parameters of CDOCKER were set by default.

2.9. Molecular Dynamics. The structure of MPH was protonated through the H++ server (https://biophysics.cs.vt.edu/) at pH 9.0. The Cd^{2+} of chain B was replaced by Zn^{2+}. Molecular dynamics (MD) was accomplished by Amber [23]. A complex of MPH and methyl-parathion/ethyl-parathion was solvated in the TIP3BOX with a minimum distance of 12 Å from the edge of the box. The force field ff14SB was applied to the system. The system was minimized through 5000 iterations by the steepest descent method and 2500 iterations by the conjugate gradient method. Then the system was heated to 300 K under Langevin control and balanced. The production phase lasted 50 ns, which was sampled every 1 ps. The interaction between enzyme and substrate was analyzed by the visualization software VMD [24]. The bonding rate was the ratio of the number of bonding frames to the total number of frames in the production phase.

2.10. Changes in Binding Free Energy. $\Delta\Delta G_{bind}$ was the difference of binding free energy (ΔGbind) between the MPH mutants and the wild type, which was calculated by Discovery Studio 2017. The force field of CHARMm Polar H was applied to the complex of MPH and substrate. The sulfur atom type of methyl-parathion and ethyl-parathion was set as "ST" which could not be identified correctly by Discovery Studio 2017. Default values were used for other parameters.

3. Results and Discussion

3.1. Improving the Catalytic Efficiency of MPH via Site-Directed Mutations. Despite lacking substrate information, the crystal structure of *Pseudomonas* sp. MPH (PDB ID: 1P9E) offered the coordinates of Zn^{2+} that are directly involved in the catalytic reactions [12]. The docking analysis using methyl-parathion as the ligand was conducted to identify those residues critical for the MPH catalytic reaction. The hydrophobic pocket with two Zn^{2+} was defined as the docking sphere with a 12.0 Å radius. The 200 docked methyl-parathions were clustered according to RMSD (root mean square deviation), and 40 poses with RMSD values higher than 4 Å were eliminated (Figure S1(a)). Based on the rest of the poses, the radius of the docking sphere was reduced to 8.5 Å and used for the next round of docking analysis. Among the 200 methyl-parathion poses, the pose that exhibited the lowest CDOCKING energy was subjected to MD analysis (Figure S1(b)), yielding the final conformation of the MPH docked with methyl-parathion (Figure 1). The 20 MPH residues within 5 Å of methyl-parathion were subjected to a virtual saturation mutation using DS calculated mutation energy (binding). As shown in Figure 2, the virtual saturation mutation induced obvious changes in binding free energy. Generally, the decrease in binding free energy of the mutants indicates a higher affinity toward the substrate, while extremely high substrate affinity may cause wrong substrate binding conformation and reduced enzyme activity [25]. To obtain the variants with improved catalytic activity, we experimentally characterized those virtual saturation mutations at L67, V97, F119, D151, T271, and T273 (Figure 2). For the virtual saturation mutation at each of these sites, the minimal binding energy change was less than −0.75 kcal/mol and over 25% of the mutations had binding energy changes below 0.

The saturation mutation at a single site of the MPH was achieved by PCR using degenerate primers (Table S1). After cyclization, the PCR products were transformed into *E. coli* BL21 (DE3), and the colonies were primarily screened in 96 wells according to the catalytic activity toward methyl-parathion or ethyl-parathion. All mutants of F119 were inactivated. The colonies with improved catalytic activity were cultivated in flasks, and the MPH mutants were purified using nickel affinity chromatography. Then, the purified MPH mutants were subjected to kinetic analysis using methyl-parathion or ethyl-parathion as the substrate (Table 1). When methyl-parathion was used as the substrate, L67, V97, and D151 mutants did not show enhanced k_{cat}/K_m. Finally, we identified two mutations at T271 benefiting the catalytic efficiency of MPH toward methyl-parathion. When methyl-parathion was used as the substrate, the k_{cat}/K_m values of the mutant T271S and T271V were 224.3% and 118.7% higher than that of the wild-type MPH, respectively. Compared to the wild-type enzyme, the K_m values of T271S and T271V were decreased by 62.2% and 60%, respectively. These results suggested the critical role of the residue 271 in the enzyme affinity against methyl-parathion. However, these mutations have little effect on the catalytic reaction toward ethyl-parathion. In contrast to the mutations at residue 271, the two mutations at residue 273 exerted significant effects on the activities against both methyl-parathion and ethyl-parathion. L273I and L273V showed 205.6% and 198.8% increases in the catalytic efficiency toward ethyl-parathion compared to the wild-type enzyme. To be noted, both the turnover number and substrate affinity (ethyl-parathion) were enhanced by introducing the mutation L273I or L273V. However, the opposite effects on the enzyme activity were observed for L273I and L273V when methyl-parathion was used as the substrate. Thus, simultaneous saturation mutations at residues 271 and 273 were conducted to further improve the activity toward both methyl-parathion and ethyl-parathion. As shown in Table 1, we obtained only one positive mutant T271S/L273V that exhibited 142.3% and 234.8% increases in the methyl-parathion- and ethyl-parathion-hydrolysis activities, respectively. Although the activity of T271S was reduced toward methyl-parathion, the double mutation T271S/L273V slightly improved the ethyl-parathion-hydrolysis activity of L273I. These results indicated that the mutations at residues 271 and 273 showed synergies in the catalytic reaction mediated by MPH. To date, there are little reports regarding the catalytic efficiency of MPH toward methyl-parathion [9, 26]. Through the random and saturation mutations of MPH from *Pseudomonas* sp. WBC-3, the mutant S277Y was obtained with a 1087.8 $mM^{-1}\,s^{-1}$ of k_{cat}/K_m toward methyl-parathion [27]. In the present study, the k_{cat}/K_m (methyl-parathion) of T271S reached 1173.4 $mM^{-1}\,s^{-1}$, suggesting a better application prospect for the latter.

3.2. Understanding the Improved Catalytic Efficiency Based on Molecular Dynamics. To understand the enhanced catalytic efficiency, the modelled structures of the T271S/methyl-parathion and L273V/ethyl-parathion complexes were built using docking and MD analysis. As shown in Figure 3, ten frames of random conformation of methyl-parathion or ethyl-parathion were selected during the MD production phase. In all the frames, both T271 and L273 did not interact with methyl-parathion in the wild-type enzyme (Figure 3(a)). Although S271 did not show any interaction with the methyl-parathion, L273 formed a hydrophobic interaction with the benzene ring of the substrate in the case of T271S (Figure 3(a)). Accordingly, RMSF (root mean square fluctuation) values of the alkyl group, nitryl group, and the whole molecule of the substrate in T271S were, respectively, lower than those in the wild-type enzyme (Figure S2). To be noted, the docked methyl-parathion was close to D151 and the water molecule that were predicted to mediate the nucleophilic attack on the phosphorus center of

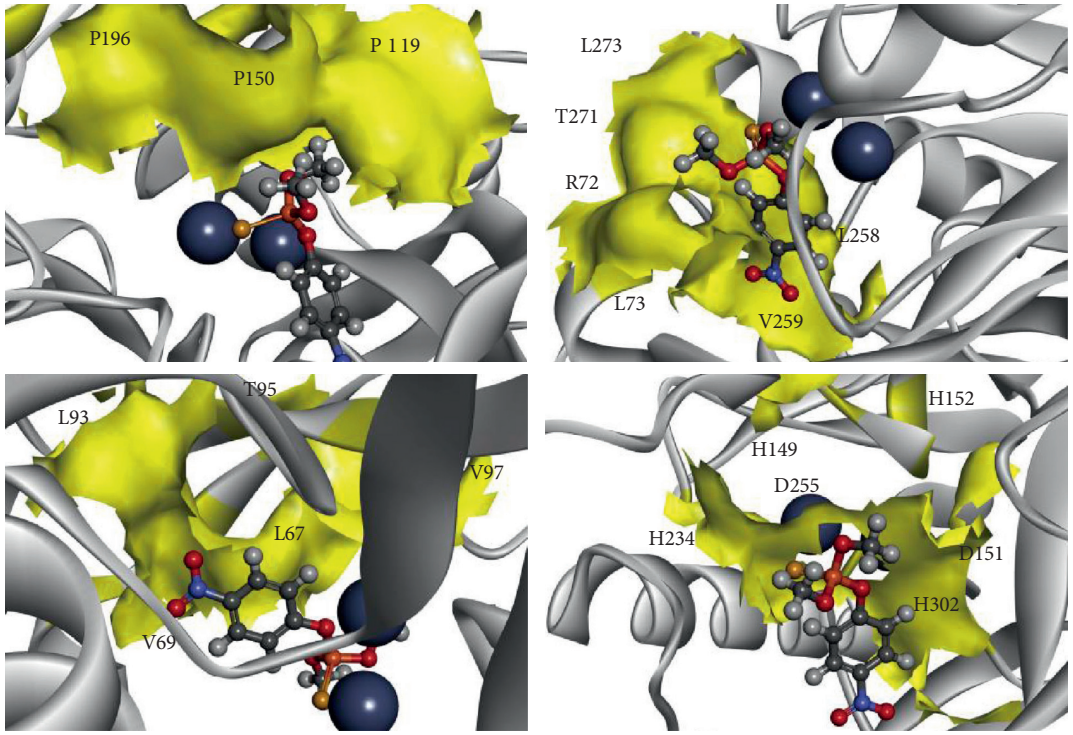

FIGURE 1: The conformation of *Pseudomonas* sp. WBC-3 MPH and the methyl-parathion complex. The MPH and methyl-parathion complex were constructed using CDOCKER of Discovery Studio, and the docking pose was further optimized by MD analysis. MPH and Zn^{2+} are shown in carton and deep purple ball, respectively. The methyl-parathion is shown in lines, while the residues within 5 Å of methyl-parathion are shown as surface in different views.

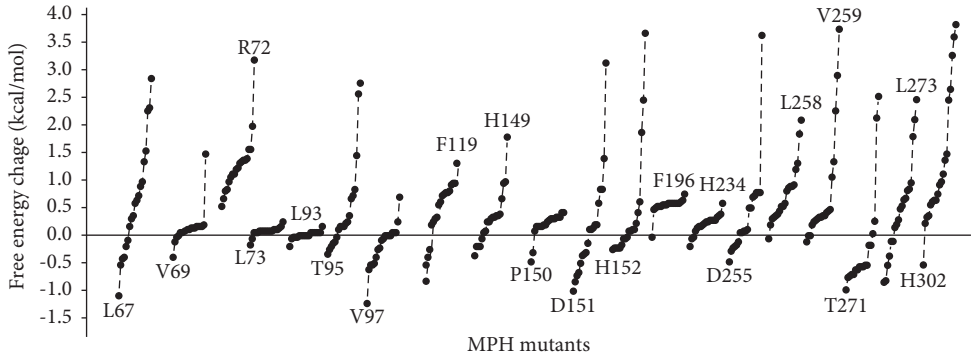

FIGURE 2: The changes in binding free energy of MPH virtual mutants. Each selected amino acid residue of MPH was replaced with the rest 19 residues, and the resulted MPH virtual mutants were subjected to docking analysis with methyl-parathion. The change in binding free energy of the corresponding enzyme-substrate complex was calculated by Discovery Studio. Each virtual mutant at a certain position was indicated by a bold dot, which was arranged according to its $\Delta\Delta G_{bind}$ value. To differentiate the positions of each mutation, the virtual mutants at the same position were connected by one dashed line.

the substrate during the catalytic process [12, 28]. The stable orientation of the substrate may be more suitable for the catalysis mediated by D151 in contrast to the less stable one. It should be noted that the K_m value of T271S was reduced compared to the wild-type enzyme. Therefore, the mutation at T271 changed the orientation of the neighboring L273, inducing an enhanced enzyme affinity toward methyl-parathion via the hydrophobic interaction (Table 1). In the case of the complexes with ethyl-parathion, both wild-type enzyme and L273V formed a hydrophobic bond between residue 273 and the substrate (Figure 3(b)). However, the formation rate of the hydrophobic interaction in the former was 32.5% higher than that in the latter, suggesting that the interaction between residue 273 and the substrate was unfavorable for the orientation and degradation of ethyl-parathion. It has been reported that the MPH showed an increase in activity toward *p*-nitrophenyl diphenyl phosphate after replacing bulky L273 with smaller alanine [14]. Considering the smaller size of leucine than that of valine, the smaller steric hindrance at 273 in L273V may account for

Table 1: Kinetic parameters of MPH mutants.

Mutants	Methyl-parathion			Ethyl-parathion		
	k_{cat} (s^{-1})	K_m (μM)	k_{cat}/K_m ($mM^{-1}s^{-1}$)	k_{cat} (s^{-1})	K_m (μM)	k_{cat}/K_m ($mM^{-1}s^{-1}$)
WT	51.9 ± 3.4	143.3 ± 11.2	361.8 ± 23.6	13.1 ± 1.8	278.3 ± 14.6	47.1 ± 7.2
L67C	5.6 ± 0.6	95.2 ± 8.4	58.8 ± 7.7	1.6 ± 0.5	681.4 ± 30.9	2.3 ± 0.9
V97A	24.4 ± 2.7	100.1 ± 9.5	242.4 ± 17.9	6.8 ± 0.8	351.4 ± 44.5	19.4 ± 4.6
D151E	21.4 ± 25.4	148.3 ± 46.5	144.3 ± 11.2	8.9 ± 1.5	124.2 ± 14.1	71.7 ± 4.3
T271S	63.6 ± 4.1	54.2 ± 8.3	1173.4 ± 53.9	15.7 ± 3.7	330.6 ± 58.5	47.5 ± 9.7
T271V	45.3 ± 3.0	57.2 ± 4.9	791.2 ± 45.4	13.9 ± 2.0	292.5 ± 27.8	49.2 ± 6.3
L273I	13.5 ± 2.7	136.4 ± 19.1	99.0 ± 5.3	32.6 ± 3.6	223.5 ± 34.5	145.8 ± 3.4
L273V	11.3 ± 1.9	186.9 ± 18.3	60.4 ± 25.5	24.3 ± 7.7	172.9 ± 5.2	140.1 ± 13.2
T271S/L273V	38.5 ± 4.8	43.9 ± 7.1	876.7 ± 67.1	20.3 ± 3.5	128.7 ± 13.8	157.7 ± 36.2
SAP3-T271S	62.9 ± 2.2	56.0 ± 3.4	1123.2 ± 26.4	12.8 ± 2.4	281.5 ± 15.6	45.5 ± 5.2

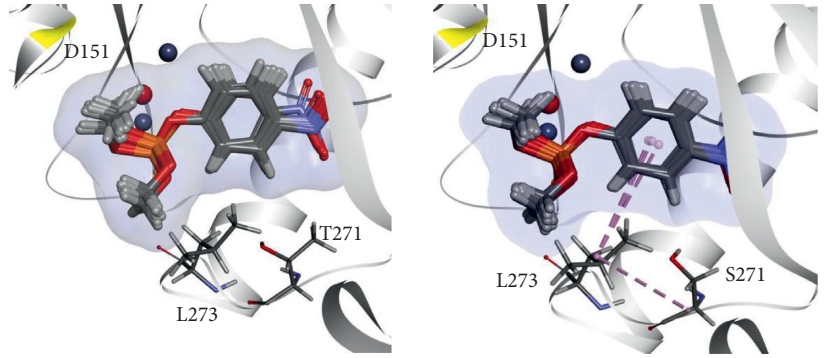

Wild-type/Methyl-parathion T271S/Methyl-parathion

(a)

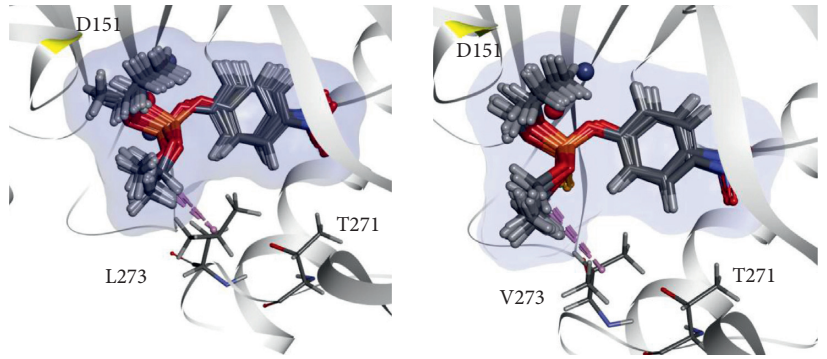

Wild-type/Ethyl-parathion L273V/Ethyl-parathion

(b)

Figure 3: The complex conformation difference between MPH and its mutant. (a) The conformation of the enzymes with methyl-parathion. (b) The conformation of the enzymes with ethyl-parathion. The enzyme-substrate complex was constructed using CDOCKER of Discovery Studio, and the docking pose was further optimized by MD analysis. The mean conformation of MPH was shown in carton. During the MD analysis, ten random samples of each substrate were selected and presented in lines. The hydrophobic bonds between enzyme and substrate were indicated by dashed lines. The active residue D151 was marked in yellow. The oxygen atoms of water and Zn^{2+} were shown as the red and deep purple balls, respectively.

its enhanced activity toward ethyl-parathion compared to the wild-type enzyme. These mechanisms could also be used to explain that the MPH activity toward ethyl-parathion was higher than that against ethyl-parathion (Table 1). In addition to the relatively smaller size than ethyl-parathion, methyl-parathion did not show any interaction with L273 (Figure 3).

3.3. Improving the Stability of MPH via the Terminal Fusion with SAP. Our previous results have indicated that fusing with SAP at the terminus could improve the enzyme thermal stability [20, 21]. To improve the thermal stability of MPH, an SAP was fused to the N- or C-terminus of MPH via a PT-Linker, and a tag with 10 histidine residues was fused at the C-terminus for affinity purification

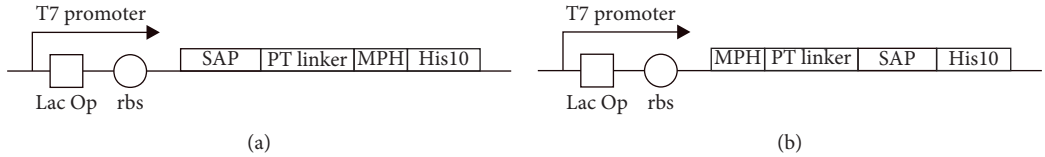

Figure 4: Expression cassettes of MPH fused with SAP. (a) SAP fused at the N-terminus of MPH via a PT-linker (PTPPTTPTPPTTPTPTP). (b) SAP fused at the C-terminus of MPH via a PT-linker. All the expression cassettes were fused with a tag composed of ten histidine residues. Six SAPs were totally used in the constructs (Table S2).

Table 2: Thermal stability parameters of MPH fused with SAP.

Fusion enzyme	T_{50} (°C)	T_m (°C)
WT	55.1	62.4
T271S	54.8	62.2
SAP1-MPH	55.5	62.4
SAP2-MPH	58.2	66.5
SAP3-MPH	61.3	68.4
SAP4-MPH	57.7	66.5
SAP5-MPH	53.7	60.6
SAP6-MPH	54.9	61.3
SAP3-T271S	59.5	67.9
MPH-SAP1	55.9	62.4
MPH-SAP2	57.2	63.7
MPH-SAP3	59.4	66.8
MPH-SAP4	56.7	64.0
MPH-SAP5	54.6	61.3
MPH-SAP6	54.3	62.2

(Figure 4). Six SAPs were tested for enhanced thermal stability (Table S2). MPH-SAP fusions were expressed intracellularly and purified after cell disruption. The T_{50} (a kinetic stability parameter that expresses the ability of an enzyme to maintain the reaction efficiency at a specific time) and T_m (a thermodynamic stability parameter that concerns the ability of an enzyme to resist the unfolding process) were used to characterize the thermal stability. Among the tested SAPs, SAP2, SAP3, and SAP4 improved the thermal stability of MPH, and fusing SAPs at the N-terminus of MPH was generally more efficient than fusion at its C-terminus (Table 2). SAP3 fused at the N-terminus of MPH (SAP3-MPH) achieved the highest thermal stability, with 6.2°C and 6.0°C increases in T_{50} and T_m than the wild-type enzyme, respectively (Table 2). However, both terminus fusion protein (SAP3-MPH-SAP3) lost its catalytic activity. The crystal structure shows that the N-terminal amino acid is no more than 5 Å away from the C-terminal amino acid of the other monomer [3], which may result in the inability to accommodate two SAPs near the end of MPH. To simultaneously improve the catalytic efficiency and stability, we fused the SAP to the N-terminus of T271S, yielding SAP3-T271S. Although less stable than SAP3-MPH, SAP3-T271S exhibited 4.4°C and 5.5°C increases in T_{50} and T_m than the wild type, respectively (Table 2). Compared with T271S, SAP3-T271S made up for the loss of stability caused by site-directed mutation (Table 2). To be noted, the SAP fusion has little impact on the activity of T271S toward methyl-parathion or ethyl-parathion (Table 2). When methyl-parathion was used as the substrate, k_{cat}/K_m of SAP-T271S was 2.1-fold higher than that of the wild-type enzyme (Table 1). As T271S did, SAP-T271S shared a similar catalytic efficiency against ethyl-parathion with the wild type.

Secondary and tertiary structure analyses of the MPH and its SAP fusions were conducted using CD (Figure 5(a)) and fluorescence spectroscopy (Figure 5(b)), respectively. However, no significant difference was observed in secondary and tertiary structure among the wild type, SAP3-MPH, and SAP3-T271S. Generally, SAP fusion was predicted to facilitate the enzyme oligomerization through intermolecular hydrophobic interactions [20, 21], which showed little impact on the secondary and tertiary structure of the enzyme [20]. Therefore, SAP3-MPH and SAP3-T271S may also adopt the same stabilization. To understand why different SAPs caused different effects on MPH, the structure of SAPs was simulated by MD (Figure S3). According to the distribution of hydrophobic and hydrophilic amino acids of SAP, the possible patterns of oligomer formation mediated by different SAPs were deduced (Figure 6). SAP1, SAP5, and SAP6 were difficult to oligomerize. SAP3 tends to form the larger scale oligomer, which provides a possible explanation for the higher stability of SAP3-MPH.

In previous studies, the T_{50} value of the MPH from *Ochrobactrum* sp. M231 was enhanced through the residue replacement with rigid proline [13] and the introduction of surface ionic bonds [29], achieving the mutant P76D/P78K with 68°C of T_{50}. However, the k_{cat}/K_m of P76D/P78K against methyl-parathion was just 178.33 $mM^{-1}s^{-1}$ [29], less than one-fifth of that of SAP-T271S. Despite being less stable than the reported mutant, SAP-T271S still showed a catalytic efficiency advantage.

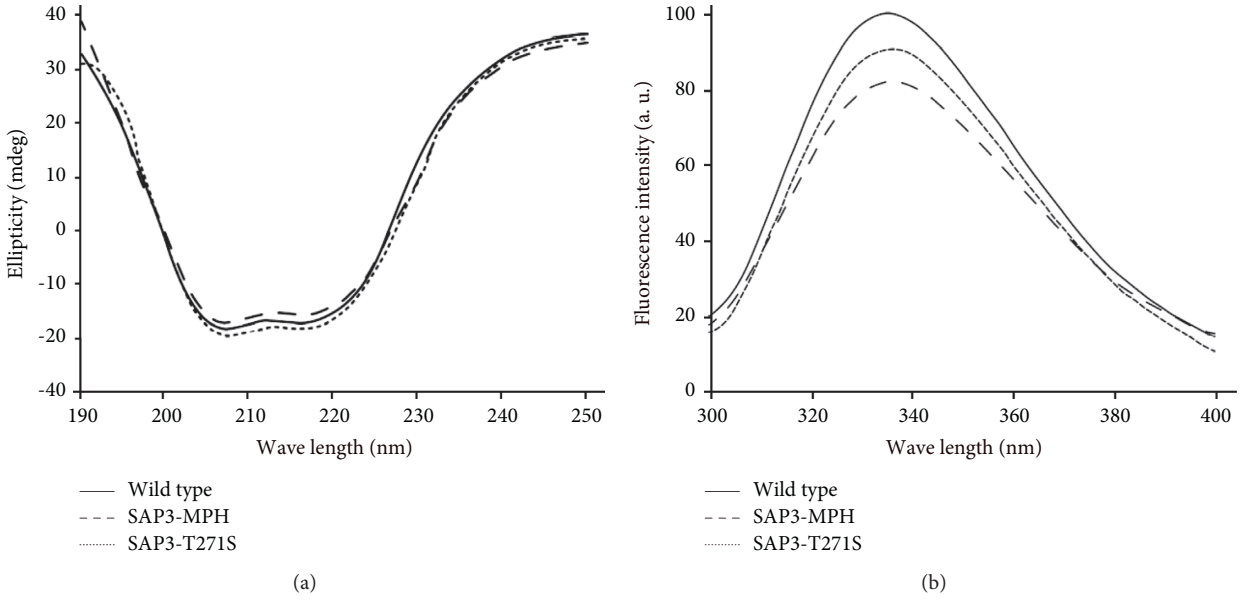

Figure 5: The effect of SAP fusion on the structure of the MPH mutants. (a) CD spectrometry. (b) Steady-state fluorescence spectra.

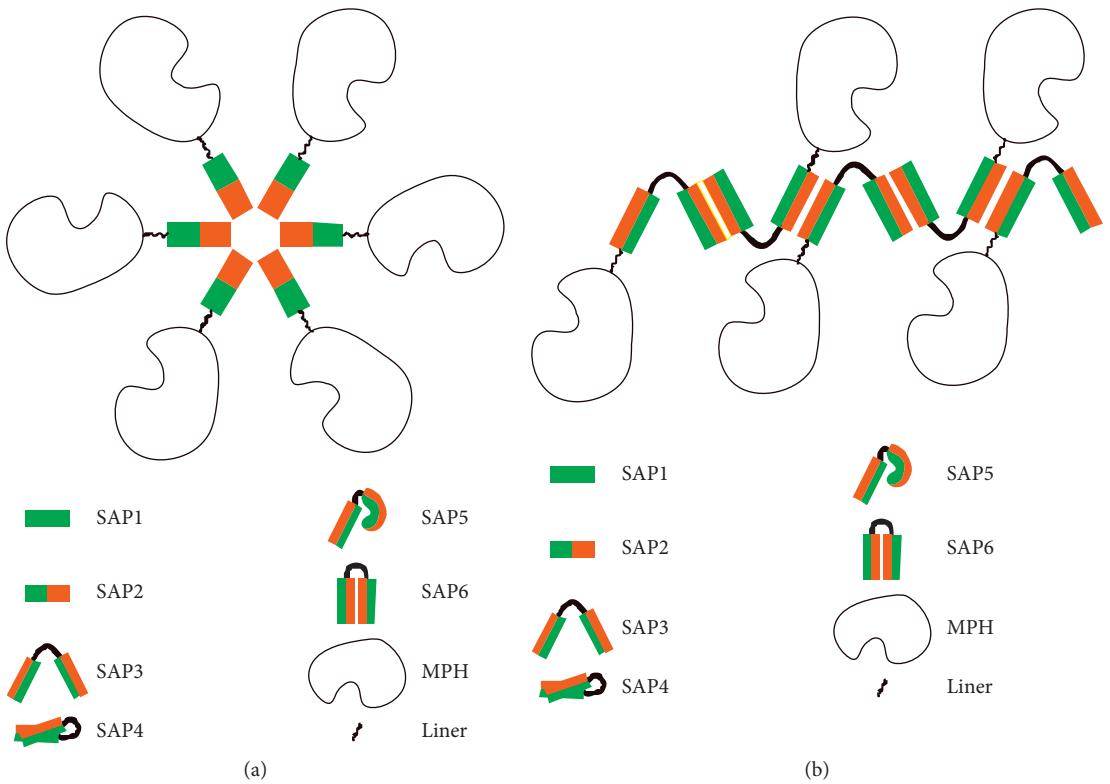

Figure 6: Continued.

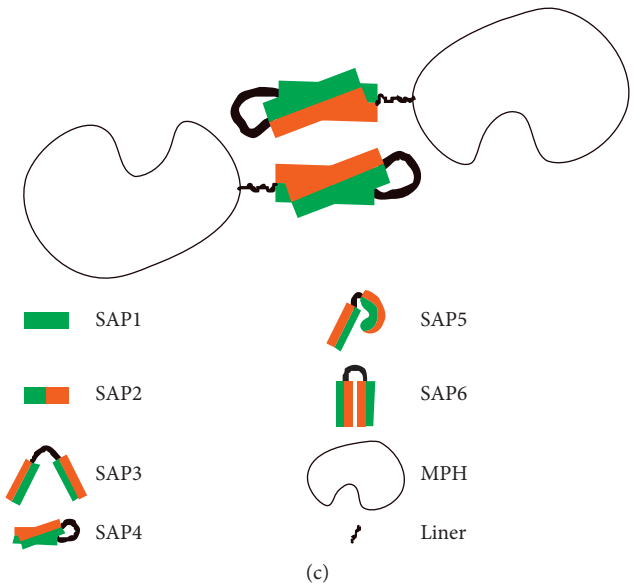

FIGURE 6: The patterns of oligomers mediated by different SAPs. The analysis of hydrophobic and hydrophilic amino acids shows the potential patterns of oligomers mediated by SAP2 (a), SAP3 (b), and SAP4 (c). The hydrophobic and hydrophilic regions are shown in brown and green, respectively.

4. Conclusion

In this study, we improved the catalytic efficiency and thermal stability of the MPH from *Pseudomonas* sp. WBC-3 using site-directed mutation and SAP fusion. Compared to the wild-type enzyme, the resulted MPH mutant SAP-T271S exhibited a 2.1-fold increase in catalytic efficiency, and it also showed 4.4°C and 5.5°C increases in T_{50} and T_m, respectively. With the improved catalytic properties, SAP-T271S could be a robust candidate for the application in the degradation and detection of organophosphorus pesticides.

Data Availability

The data used to support the findings of this study are included within the article and supplementary information file.

Ethical Approval

This article does not contain any studies with human participants or animals performed by any of the authors.

Conflicts of Interest

The authors declare that they have no competing interests.

Authors' Contributions

Cheng Shi, Song Liu, Guocheng Du, Song Liu, and Guocheng Du conceived and designed the research; Cheng Shi and Song Liu performed the experiments; Cheng Shi and Song Liu analyzed the data; Cheng Shi and Song Liu contributed the reagents/materials/analytical tools; Cheng Shi, Guocheng Du, and Song Liu wrote the paper All authors have read and approved the final manuscript for publication.

Acknowledgments

This work was financially supported by the National Key Research and Development Program of China (2019YFA0905300), the National Natural Science Foundation of China (32071474), Fundamental Research Funds for the Central Universities (JUSRP52026A), and Scientific and Technological Innovation Major Base of Guangxi (2018-15-Z03).

Supplementary Materials

Table S1: primers in this study. Table S2: SAPs used in this study. Figure S1: docking poses of methyl-parathion in *Pseudomonas* sp. WBC-3 MPH. (a) Docking in the sphere with a 12.0 Å radius. (b) Docking in the sphere with an 8.5 Å radius. For each docking result, 200 poses were clustered into Group 1 and Group 2 according to their RMSD values. All of the docking analyses were conducted using CDOCKER of Discovery Studio. Figure S2: RMSF of substrate in *Pseudomonas* sp. WBC-3 MPH and its mutants during the MD production phase. The enzymes docked with substrate (wild type/methyl-parathion, wild type/ethyl-parathion, T271S/methyl-parathion, and L273V/ethyl-parathion) were subjected to MD analysis, respectively. The RMSF of the whole substrate, alkyl group, and nitrobenzol group of the substrate during the MD production phase was calculated using Amber. Figure S3: three-dimensional structure of SAP monomers. The structure of the SAP monomer was simulated by MD. SAP was shown in cartoon and surface. The surface was colored by the hydrophobicity of amino acids. (*Supplementary Materials*)

References

[1] T. A. d. F. Matos, A. L. N. Dias, A. D. P. Reis, M. R. A. d. Silva, and M. M. Kondo, "Degradation of abamectin using the photo-fenton process," *International Journal of Chemical Engineering*, vol. 2012, Article ID 915724, 2012.

[2] F. Sadeghi, A. Fadaei, F. Mohammadi-Moghadam, S. Hemati, and G. Mardani, "Photocatalytic degradation of trifluralin in aqueous solutions by UV/S2O82− and UV/ZnO processes: a comparison of removal efficiency and cost estimation," *International Journal of Chemical Engineering*, vol. 2021, 2021.

[3] Y.-J. Dong, M. Bartlam, L. Sun et al., "Crystal structure of methyl parathion hydrolase from *Pseudomonas* sp. WBC-3," *Journal of Molecular Biology*, vol. 353, no. 3, pp. 655–663, 2005.

[4] C. M. Theriot and A. M. Grunden, "Hydrolysis of organophosphorus compounds by microbial enzymes," *Applied Microbiology and Biotechnology*, vol. 89, no. 1, pp. 35–43, 2011.

[5] W. Yang, Y.-F. Zhou, H.-P. Dai et al., "Application of methyl parathion hydrolase (MPH) as a labeling enzyme," *Analytical and Bioanalytical Chemistry*, vol. 390, no. 8, pp. 2133–2140, 2008.

[6] W. Song, H.-J. Zhang, Y.-H. Liu, C.-L. Ren, and H.-L. Chen, "A new fluorescence probing strategy for the detection of parathion-methyl based on N -doped carbon dots and methyl parathion hydrolase," *Chinese Chemical Letters*, vol. 28, no. 8, pp. 1675–1680, 2017.

[7] W. Ying, W. YaPing, H. Can et al., "High-level extracellular production and immobilisation of methyl parathion hydrolase from Plesiomonas sp. M6 expressed in *Pichia pastoris*," *Protein Expression and Purification*, vol. 183, Article ID 105859, 2021.

[8] G. Gotthard, J. Hiblot, D. Gonzalez, M. Elias, and E. Chabriere, "Structural and enzymatic characterization of the phosphotriesterase OPHC2 from *Pseudomonas pseudoalcaligenes*," *PLoS One*, vol. 8, no. 11, Article ID e77995, 2013.

[9] X.-Y. Liu, F.-F. Chen, C.-X. Li et al., "Improved efficiency of a novel methyl parathion hydrolase using consensus approach," *Enzyme and Microbial Technology*, vol. 93-94, pp. 11–17, 2016.

[10] X.-X. Wang, Z. Chi, S.-G. Ru, and Z.-M. Chi, "Genetic surface-display of methyl parathion hydrolase on *Yarrowia lipolytica* for removal of methyl parathion in water," *Biodegradation*, vol. 23, no. 5, pp. 763–774, 2012.

[11] J. Xie, H. Zhang, X. Li, and Y. Shi, "Entrapment of methyl parathion hydrolase in cross-linked poly (γ-glutamic acid)/gelatin hydrogel," *Biomacromolecules*, vol. 15, no. 2, pp. 690–697, 2014.

[12] A. N. Bigley and F. M. Raushel, "Catalytic mechanisms for phosphotriesterases," *Biochimica et Biophysica Acta (BBA)-Proteins and Proteomics*, vol. 1834, no. 1, pp. 443–453, 2013.

[13] J. Tian, P. Wang, S. Gao, X. Chu, N. Wu, and Y. Fan, "Enhanced thermostability of methyl parathion hydrolase from *Ochrobactrum* sp. M231 by rational engineering of a glycine to proline mutation," *FEBS Journal*, vol. 277, no. 23, pp. 4901–4908, 2010.

[14] Y.-S. Jeong, S.-L. Choi, H.-H. Kyeong et al., "High-throughput screening system based on phenolics-responsive transcription activator for directed evolution of organophosphate-degrading enzymes," *Protein Engineering Design and Selection*, vol. 25, no. 11, pp. 725–731, 2012.

[15] R. Chowdhury and C. D. Maranas, "From directed evolution to computational enzyme engineering—a review," *AIChE Journal*, vol. 66, no. 3, Article ID e16847, 2020.

[16] J. Tirado-Rives and W. L. Jorgensen, "Contribution of conformer focusing to the uncertainty in predicting free energies for Protein–Ligand binding," *Journal of Medicinal Chemistry*, vol. 49, no. 20, pp. 5880–5884, 2006.

[17] Z. Cournia, B. Allen, and W. Sherman, "Relative binding free energy calculations in drug Discovery: recent advances and practical considerations," *Journal of Chemical Information and Modeling*, vol. 57, no. 12, pp. 2911–2937, 2017.

[18] D. Hao, X. He, B. Ji, S. Zhang, and J. Wang, "How well does the extended linear interaction energy method perform in accurate binding free energy calculations?" *Journal of Chemical Information and Modeling*, vol. 60, no. 12, pp. 6624–6633, 2020.

[19] R. Han, X. Cao, H. Fang, J. Zhou, and Y. Ni, "Structure-based engineering of ω-transaminase for enhanced catalytic efficiency toward (R)-(+)-1-(1-naphthyl)ethylamine synthesis," *Molecular Catalysis*, vol. 502, Article ID 111368, 2021.

[20] X. Lu, S. Liu, D. Zhang et al., "Enhanced thermal stability and specific activity of *Pseudomonas aeruginosa* lipoxygenase by fusing with self-assembling amphipathic peptides," *Applied Microbiology and Biotechnology*, vol. 97, no. 21, pp. 9419–9427, 2013.

[21] W. Zhao, G. Du, and S. Liu, "An efficient thermostabilization strategy based on self-assembling amphipathic peptides for fusion tags," *Enzyme and Microbial Technology*, vol. 121, pp. 68–77, 2019.

[22] C. Shi, S. Liu, and G. Du, "CityApps: a bioinformatics tool for predicting the key residues of enzymes weakly interacting with monovalent metal ions," *Process Biochemistry*, vol. 104, pp. 76–82, 2021.

[23] R. Salomon-Ferrer, D. A. Case, and R. C. Walker, "An overview of the Amber biomolecular simulation package," *WIREs Computational Molecular Science*, vol. 3, no. 2, pp. 198–210, 2013.

[24] W. Humphrey, A. Dalke, and K. Schulten, "VMD: visual molecular dynamics," *Journal of Molecular Graphics*, vol. 14, no. 1, pp. 33–38, 1996.

[25] J. Bi, H. Xia, F. Li, X. Zhang, and Y. Li, "The effect of U1 snRNA binding free energy on the selection of 5′ splice sites," *Biochemical and Biophysical Research Communications*, vol. 333, no. 1, pp. 64–69, 2005.

[26] J. Xie, Y. Zhao, H. Zhang, Z. Liu, and Z. Lu, "Improving methyl parathion hydrolase to enhance its chlorpyrifos-hydrolysing efficiency," *Letters in Applied Microbiology*, vol. 58, no. 1, pp. 53–59, 2014.

[27] Y. Li, H. Yang, and F. Xu, "Identifying and engineering a critical amino acid residue to enhance the catalytic efficiency of *Pseudomonas* sp. methyl parathion hydrolase," *Applied Microbiology and Biotechnology*, vol. 102, no. 15, pp. 6537–6545, 2018.

[28] M. Purg, A. Pabis, F. Baier, N. Tokuriki, C. Jackson, and S. C. L. Kamerlin, "Probing the mechanisms for the selectivity and promiscuity of methyl parathion hydrolase," *Philosophical Transactions of the Royal Society A: Mathematical, Physical and Engineering Sciences*, vol. 374, no. 2080, Article ID 20160150, 2016.

[29] Y. Su, J. Tian, P. Wang et al., "Improving the thermostability of a methyl parathion hydrolase by adding the ionic bond on protein surface," *Applied Biochemistry and Biotechnology*, vol. 165, no. 3-4, pp. 989–997, 2011.